Journal of Nuclear Materials 449 (2014) 252–262

Contents lists available at ScienceDirect

Journal of Nuclear Materials

journal homepage: www.elsevier.com/locate/jnucmat

Dislocation dynamics simulations of interactions between gliding dislocations and radiation induced prismatic loops in zirconium

Julie Drouet [a,*], Laurent Dupuy [a], Fabien Onimus [a], Frédéric Mompiou [b], Simon Perusin [c], Antoine Ambard [d]

[a] Service de Recherches Métallurgiques Appliquées, CEA-Saclay, 91191 Gif-sur-Yvette, France
[b] CEMES-CNRS and Université de Toulouse, 29 Rue Jeanne Marvig, 31055 Toulouse Cedex 4, France
[c] AREVA NP SAS Fuel Business Unit 10, Rue Juliette Recamier, 69456 Lyon Cedex 06, France
[d] EDF/R&D Les Renardières, Ecuelles, 77818 Moret sur Loing Cedex, France

ARTICLE INFO

Article history:
Available online 8 December 2013

ABSTRACT

The mechanical behavior of Pressurized Water Reactor fuel cladding tubes made of zirconium alloys is strongly affected by neutron irradiation due to the high density of radiation induced dislocation loops. In order to investigate the interaction mechanisms between gliding dislocations and loops in zirconium, a new nodal dislocation dynamics code, adapted to Hexagonal Close Packed metals, has been used. Various configurations have been systematically computed considering different glide planes, basal or prismatic, and different characters, edge or screw, for gliding dislocations with ⟨a⟩-type Burgers vectors. Simulations show various interaction mechanisms such as (i) absorption of a loop on an edge dislocation leading to the formation of a double super-jog, (ii) creation of a helical turn, on a screw dislocation, that acts as a strong pinning point or (iii) sweeping of a loop by a gliding dislocation. It is shown that the clearing of loops is more favorable when the dislocation glides in the basal plane than in the prismatic plane explaining the easy dislocation channeling in the basal plane observed after neutron irradiation by transmission electron microscopy.

1. Introduction

Zirconium alloys are widely used in nuclear industry as constitutive material of the fuel cladding tubes of Pressurized Water Reactors [1]. Submitted to radiation during in-reactor use, the mechanical behavior of the material undergoes significant changes, such as strengthening and early plastic instability due to low strain hardening capability [2].

At the microscopic scale fast neutron irradiation creates a high density of small point defect clusters in the form of dislocation loops. These small loops have a ⟨a⟩ Burgers vector and are located in the prismatic planes of the Hexagonal Close Packed (HCP) structure of zirconium [2–6]. There are several evidences that the loops are mainly non-edge, the habit plane being tilted towards the $\{1\bar{1}00\}$ planes. Both vacancy and interstitial ⟨a⟩ loops can be found at the same time in the material depending on irradiation conditions. The three loop populations (three ⟨a⟩ Burgers vectors are possible in the HCP structure) are also found in the same proportion [7]. Furthermore, these ⟨a⟩ loops are perfect and can therefore glide on their cylinder.

These loops act as obstacles to dislocation glide explaining the radiation induced hardening at the macroscopic scale [8,9]. Indeed, when a gliding dislocation encounters a loop, a junction can be created which constitutes a pinning point for the gliding dislocation [8,10–12]. However, it is also seen that for a sufficient applied stress the loops can be cleared by gliding dislocations, following various interaction mechanisms [8,11–14], creating a defect free channel, or clear band, where further dislocations can glide easily [14–18]. This microscopic strain softening explains the low strain hardening capability and therefore the early strain localization observed at the macroscopic scale.

In the case of zirconium alloys, defect free channels have been observed by many authors [19–25]. More recently a thorough study of the dislocation channeling mechanism and of the activated slip systems after neutron irradiation at 20 °C and 350 °C has been performed in zirconium alloys [26–29]. It has been clearly demonstrated that, although glide occurs primarily in prismatic systems in the unirradiated material, basal systems become the preferable slip systems after irradiation. This change of the easy glide slip system has been attributed, based on theoretical considerations [26,30], to differences in interactions between irradiation loops and dislocations gliding either in the basal plane or in the prismatic plane. This simple theoretical analysis, based on line tension approximation, compares well with experimental results, but

* Corresponding author.
E-mail address: julie.drouet@cea.fr (J. Drouet).

0022-3115/$ - see front matter © 2013 Elsevier B.V. All rights reserved.
http://dx.doi.org/10.1016/j.jnucmat.2013.11.049

still remains insufficiently accurate. Indeed, this approach does not take into account the long range elastic interactions between dislocations and loops that can significantly modify the resulting mechanism. Furthermore, with this approach it is not possible to study systematically the effect of the relative position of the loop with respect to the dislocation or interactions involving several loops. Moreover, quantitative estimation of the interaction strength is not achievable with this method.

In order to gain a better understanding and prediction of elementary interactions between gliding dislocations and radiation induced loops, and also of the dislocation channeling process, numerical simulations at various length scales, such as Molecular Dynamics (MD) or discrete Dislocation Dynamics (DD), are needed for zirconium.

MD simulations have now been used for more than ten years, by many authors [31–45], to study interactions between dislocation and point defect clusters such as Stacking Fault Tetrahedron, voids or dislocation loops. In their two recent reviews, Osetsky, Bacon and Rodney [46,47] have described in details the various interactions observed in Face Centered Cubic (FCC) and Body Centered Cubic (BCC) metals. Concerning HCP metals, Voskoboynikov et al. [48,49] have performed MD simulations of interactions between gliding dislocations and small point defect clusters in zirconium, using the interatomic potential developed by Ackland et al. [50]. During the reviewing process of the present article, Serra and Bacon [51] have investigated at atomic level the interaction between small interstitial ⟨a⟩ loops and dislocations gliding in prismatic planes. The reaction mechanisms observed at MD scale are in global agreement with our findings.

At a larger length scale, some authors [52–55] have used discrete DD simulations to study junctions between two dislocations in HCP materials. DD simulations of irradiated FCC metals have also been performed [56–58] to study plastic flow localization at the grain scale using simplified treatments for the elementary dislocation-loops interactions. More recently Arsenlis et al. [59] have performed advanced DD computations of heterogeneous deformation in irradiated BCC iron taking into account the full details of dislocation loops interactions. In the case of HCP metals, no such computation is available yet.

Here we report the use of the DD code NUMODIS, based on the nodal topology and adapted to HCP metals, to compute dislocation-loop interaction in irradiated zirconium and investigate its behavior.

After this introduction, the new nodal DD code NUMODIS is described. In a third part the method, geometry and parameters are detailed. In a fourth part, the results of the simulations are presented. Following an approach similar to MD simulations, elementary interactions between prismatic ⟨a⟩ dislocation loops and edge or screw ⟨a⟩ dislocations, gliding in the prismatic or basal planes of the HCP lattice have been systematically computed. In the fifth part of the paper, the results obtained are discussed in light of other simulation results and experimental works.

2. Dislocation dynamics code: NUMODIS

Numerical dislocation dynamics simulations were performed using a new discrete Dislocation Dynamics code, NUMODIS (Numerical Modelling of Dislocations), developed in France at CEA (Saclay) in collaboration with CNRS (Grenoble and Thiais) and INRIA (Bordeaux).[1] This code bears similarities with the code ParaDiS (Parallel Dislocation Simulator) developed in the USA at Lawrence Livermore National Laboratory and Standford University. It is based on a nodal representation [60–62] where the dislocation lines are discretized into a serie of inter-connected linear segments. In the present study, a Burgers vector and a glide plane are attributed to each segment. This representation requires a limited number of degrees of freedom while adequately capturing the general dislocation line topology including all possible junctions. The NUMODIS code has been developed to treat BCC, FCC as well as HCP crystal structures. The HCP structure is taken into account explicitly and the four Miller-Bravais indices are used in the computation. This code is therefore well suited to address the plasticity of irradiated zirconium.

The forces acting at each end nodes of the discrete dislocation segments (nodal forces) are computed, using formulae described by Arsenlis et al. [62], as the negative derivative of the stored energy in the system with respect to the positions of each node. The total stored energy is partitioned into two parts: the core energy, associated with the local atomic configuration of the dislocation cores, and the elastic energy associated with the long range elastic distortion. The approach chosen here for the computation of the elastic energy is the non-singular continuum elastic theory of dislocations proposed by Cai et al. [63]. This theory is capable of describing the forces acting on all points in the discrete network. The cut-off radius is chosen equal to one Burgers vector of ⟨a⟩-type dislocations ($r_c = a$). As pointed out in [62] the core energy contributions to self-energy play an important role in the formation and breaking of dislocation junctions and is therefore essential in the case of this study.

With the nodal forces determined, the nodal equations of motion are completed by specifying the nodal velocity as a function of the nodal forces. Here a simple linear mobility law is chosen for dislocation glide (Eq. (1)). No dislocation climb or cross-slip is taken into account in the present study. Obviously, motion of a discretization node along the line direction has no physical significance. In order to prevent this motion a tangential viscosity is introduced (with $B_{tangent} = B_{glide}/10$).

With these mobility laws, the nodal velocities are then computed by solving the full linear system, as described in [62]. Then an explicit time integrator is used to update the position of each node. Topological changes such as remeshing, merging and splitting of multi-arm nodes have been introduced using algorithms similar to the ParaDiS code. Particular attention has been given to the node splitting algorithm, which allows multi-arms nodes to split into several nodes by selecting the junction reaction that maximizes the energy reduction rate as described in [3]. All dislocation segments being constrained by their glide plane, it should be mentioned that nodes with three arms are possible candidates for the splitting operation. These nodes can indeed split into two nodes connected by a junction whose Burgers vector is identical to the isolated original arm but whose glide plane is different. As shown in the following, this mechanism, which presents strong similarities with cross-slip, plays an important role in some reactions between dislocation and radiation induced loops. Details about this splitting algorithm will be published in a separate article.

3. Method, geometry, loading conditions and parameters

3.1. Loop geometry

In the present investigation, radiation induced ⟨a⟩ loops are considered, as represented in Fig. 1, as a simplified closed squared dislocation lying in one of the three second order prismatic plane noted $P_{L1} = (11\bar{2}0)$ for the loop of type 1 (respectively,

[1] See http://www.numodis.com.

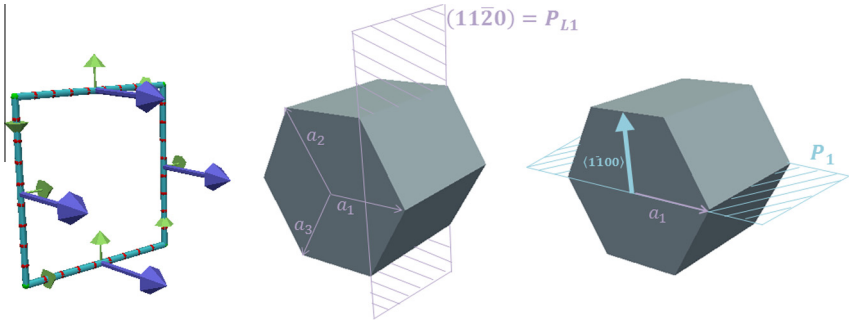

Fig. 1. Schematic representation of a vacancy loop with the Burgers vector $\underline{b}_L = \underline{a}_1$, in the P_{L1} plane. Blue arrows correspond to the Burgers vectors of the loop, green arrows are the normal to the glide planes of each segment and their line orientation. P_{Ln} planes are the second order prismatic planes, and P_n planes are the first order prismatic planes. Dislocation segments can thus glide either in the P_n planes or in the basal plane $B = (0001)$. (For interpretation of the references to color in this figure legend, the reader is referred to the web version of this article.)

$P_{L2} = (\bar{2}110)$ $P_{L3} = (1\bar{2}10)$ for loops of type 2 and 3). Although ⟨a⟩ loops are experimentally also found in first order prismatic planes [3,4], such loops would, in our model, not correspond to an energetically favorable configuration and they would therefore tilt in second order prismatic planes.

The four segments have the same Burgers vector (referred as $\underline{b}_L$ following Carpenter's conventions [64]), perpendicular to the loop plane, i.e. $\underline{a}_1 = \frac{1}{3}[11\bar{2}0]$ (resp. $\underline{a}_2 = \frac{1}{3}[\bar{2}110]$, $\underline{a}_3 = \frac{1}{3}[1\bar{2}10]$). In Fig. 1, two segments of the loop are assigned to the first order prismatic plane $P_1 = (1\bar{1}00)$ (resp. $P_2 = (01\bar{1}0)$, $P_3 = (10\bar{1}0)$), while the two other segments are assigned to the basal plane $B = (0001)$. The loop size is chosen as a square of d =10 nm side length. This value is in agreement with the TEM observations on neutron irradiated zirconium (d = 8 nm from [27], d = 14 nm from [65]).

Since in zirconium both vacancy and interstitial loops can be present, simulations with both types of loops have been performed. In the following, only interactions with vacancy loops are presented. According to the FS/RH convention, which applies in the NUMODIS code, the Burgers vector of a vacancy loop is in the same direction as the normal to the loop plane as defined by the Right Hand circuit convention (see Fig. 1). In the following, blue arrows represent the Burgers vector of the dislocation, and green arrows are the normal to the glide planes as well as dislocation orientations. Note that ⟨c⟩-component loops were not considered in this study.

3.2. Initial configuration

An initial Frank-Read source of 350 nm length is introduced in the simulation box. Both extremities of this dislocation are pinned. Five dislocation loops are then introduced 10 nm ahead and parallel to the Frank-Read source (i) as a surrogate to periodic boundary conditions and (ii) to break the symmetry (and possible artifacts) of a periodic system containing a single loop. The glide plane of the Frank-Read source crosses the center of each loop. In order to be representative of the microstructure observed after neutron irradiation (loop density being $N = 2\text{–}5 \times 10^{22}$ m^{-3}), the distance between the center of each loop is chosen to be L = 50 nm. This corresponds to a loop number density of $N = 1/L^3 = 0.8 \times 10^{22}$ m^{-3}. For the sake of clarity, visualization snapshots are focused on a single loop.

In all computations, the dislocation has always $\underline{b}_G = \underline{a}_1$ Burgers vector. The dislocation is either screw or edge and can either glide in the prismatic plane $P_1 = (1\bar{1}00)$ or in the basal plane $B = (0001)$. In this study, we did not consider pyramidal planes as possible glide planes, nor dislocation with ⟨c + a⟩ Burgers vector.

3.3. Mechanical loading

Dislocation and loops are submitted to a constant shear stress during the entire simulation, equivalent to a creep-like mechanical loading. Pure shear is applied in the glide plane of the dislocation, P_1 or B, in the direction of its Burgers vector $\underline{b}_G = \underline{a}_1$, resulting in a resolved shear stress τ of 100 MPa, corresponding to typical stress levels investigated using molecular dynamics [46]. Depending on the reaction outcome, lower and higher stress levels are considered although no attempt is made in this study to measure quantitatively the critical resolved shear stress to overcome a radiation induced loop.

3.4. Physical parameters

In the simulation, typical values of the lattice parameters of zirconium (a = 3.233 Å and c = 5.147 Å) are taken. The elasticity coefficients are taken to be E = 80 GPa at 350 °C, according to Northwood and Rosinger [66] and the Poisson's ratio is taken as ν = 0.4 according to [67].

The mobility law chosen for dislocation velocity is the usual phonon drag law given in Eq. (1) (v is the steady state velocity, τ^* is the resolved effective stress, and b is the Burgers vector). The viscous drag coefficient is taken as B_{glide} = 100 μPa s, which is close to typical values used in MD simulations (1–100 μPa s). This high value of the viscous drag coefficient can account for the effect of alloying elements that imped the dislocation glide.

$$v = \frac{\tau^* b}{B_{glide}} \tag{1}$$

In the following, different cases of interactions between dislocations and loops are considered.

4. Results

4.1. Dislocations gliding in a prismatic plane

(i) Edge dislocation gliding in a prismatic plane interacting with a loop with the same Burgers vector

An edge dislocation gliding in the P_1 prismatic plane with a $\underline{b}_G = \underline{a}_1$ Burgers vector interacts with a vacancy loop located in the P_{L1} prismatic plane with a $\underline{b}_L = -\underline{a}_1$ Burgers vector (Fig. 2(a)).

Under a constant resolved shear stress (τ = 100 MPa) in the P_1 prismatic plane along the $\underline{a}_1$ direction, the dislocation starts to glide. The two opposite segments of the loop lying in P_1 prismatic planes also undergo a Peach-Koehler force due to the applied shear

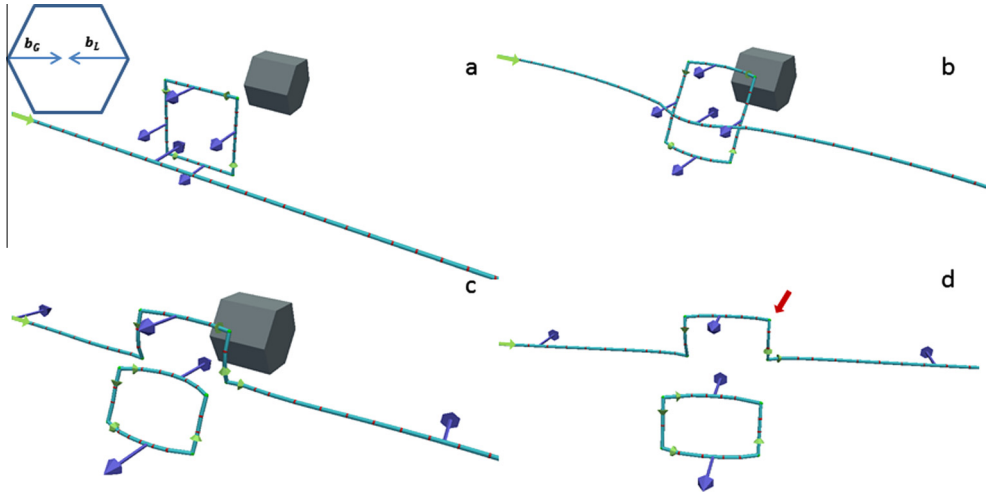

Fig. 2. Interaction between an edge dislocation $\underline{b}_G = \underline{a}_1$ gliding in a prismatic plane and a loop $\underline{b}_L = \underline{a}_1$ with opposite Burgers vectors. The applied stress in the gliding plane of the dislocation is $\tau = 100$ MPa, allowing a double super-jog (pointed out by the red arrow on (d)) to be formed on the dislocation line. (For interpretation of the references to color in this figure legend, the reader is referred to the web version of this article.)

stress and therefore tend to glide. However due to the opposite line orientations, the Peach–Koehler force acts in opposite directions inducing a tilt of the loop (Fig. 2(b)). This tilt is nevertheless balanced by the increase of dislocation length, the loop reaching therefore an equilibrium position.

An elastic repulsive interaction is also observed when the dislocation approaches the loop. This is due to the elastic repulsion between the dislocation and the segment of the loop gliding in the P_1 prismatic plane that has the same line orientation and Burgers vector as the dislocation.

From the simulation, it can be seen that the interaction depends on the magnitude of the applied resolved shear stress. Indeed for low stress values (50 MPa typically here), the elastic repulsive interaction predominates, pushing the loop along its glide cylinder and slowing down the dislocation glide. This phenomenon depends on the magnitude of the viscous drag coefficient (B_{glide}) and on the magnitude of the applied stress. Indeed, for high B_{glide} values or if the applied stress is sufficient to overcome the elastic repulsive interaction ($\tau = 100$ MPa with $B_{glide} = 100$ μPa s), a double super-jog is formed on the edge dislocation and a part of the loop is then left out after the interaction (Fig. 2(c and d)). The dragging of these jogs on the dislocation leads to a reduction of its mobility of about 10% in the present case. This type of reaction has been described by Saada and Washburn [12] and analyzed for zirconium in [30]. In the notation proposed by Bacon et al. [46], this interaction is referred to as the *R*3 reaction, which consists of a partial or full absorption of the loop by an edge dislocation that acquires a double super-jog. This reaction can be interpreted as a collinear annihilation between two dislocations with the same Burgers vector, as described in [68].

It has also to be pointed out that when the loop is of interstitial type, the direction of the loop line is reversed, resulting in a double super-jog below the gliding plane of the dislocation shown in Fig. 2.

(ii) Edge dislocation gliding in a prismatic plane interacting with a loop with a different Burgers vector

An edge dislocation gliding in the P_1 prismatic plane with a $\underline{b}_G = \underline{a}_1$ Burgers vector interacts with a vacancy loop located in the P_{L3} plane with a $\underline{b}_L = \underline{a}_3$ Burgers vector (Fig. 3(a)).

Under the applied stress ($\tau = 100$ MPa), the dislocation glides towards the loop. Due to attractive long range elastic interaction, the dislocation and the loop glide towards each other and form a junction with a Burgers vector $\underline{b}_J = \underline{a}_2$ gliding in the P_2 prismatic plane (Fig. 3(b)). On the figures given in the following, an hexagon shows the Burgers vectors of the dislocations involved in the junction formation. The represented Burgers vectors are taken with respect to the line directions, their sum being zero at triple nodes [64]. The Burgers vector of the junction is thus given by Eq. (2).

$$\underline{b}_J = -(\underline{b}_G + \underline{b}_L) = -(\underline{a}_1 + \underline{a}_3) = \underline{a}_2 \tag{2}$$

The entire loop progressively tilts in the junction plane as it glides further away. Simultaneously, the junction glides and changes the Burgers vectors of the two arms of the loop located in the basal plane, which become $\underline{a}_1$ (Fig. 3(c)). When the junction in the P_2 prismatic plane reaches the top side of the loop, it reacts forming another junction with Burgers vector $\underline{a}_1$, Burgers vector which can glide in the P_1 prismatic plane. Indeed the Burgers vector of the resulting "junction" ($\underline{b}'_J$) is:

$$\underline{b}'_J = -(\underline{b}_J + \underline{b}_L) = -(\underline{a}_2 + \underline{a}_3) = \underline{a}_1 \tag{3}$$

The whole interaction mechanism leads therefore to the formation of a double super-jog on the edge gliding dislocation (Fig. 3(d)). Contrary to the case described in Fig. 2, the loop is completely erased by this mechanism, also referred as *R*3 reaction in [46]. It has also been observed in MD simulations in iron by [43], and in zirconium by Voskoboynikov et al. [48] although intermediate configurations are not given in this latter case.

This reaction can also be analyzed by considering the interactions between two non-coplanar dislocations as studied by several authors [52–54,69,70] for HCP materials and represented as interaction maps. In these interaction maps, the line orientations of the two dislocations are defined by their angles Φ_1 and Φ_2 with respect to the intersection direction between the two slip systems. For each Φ_1 and Φ_2, the nature of the interaction is considered either as a repulsive, attractive (causing the formation of a junction) or a crossed state which is the pinning of the dislocations when the formation of a junction is not energetically favorable [71]. Monnet et al. [52] have established an interaction map between two non-coplanar dislocations in zirconium involving two dislocations in two different prismatic planes. Wu et al. [53] have performed the same computation in beryllium for a dislocation gliding in the basal plane and another in a prismatic plane. Recently, Devincre [54], in the case of ice, has added to these results interaction maps for basal–pyramidal slip systems,

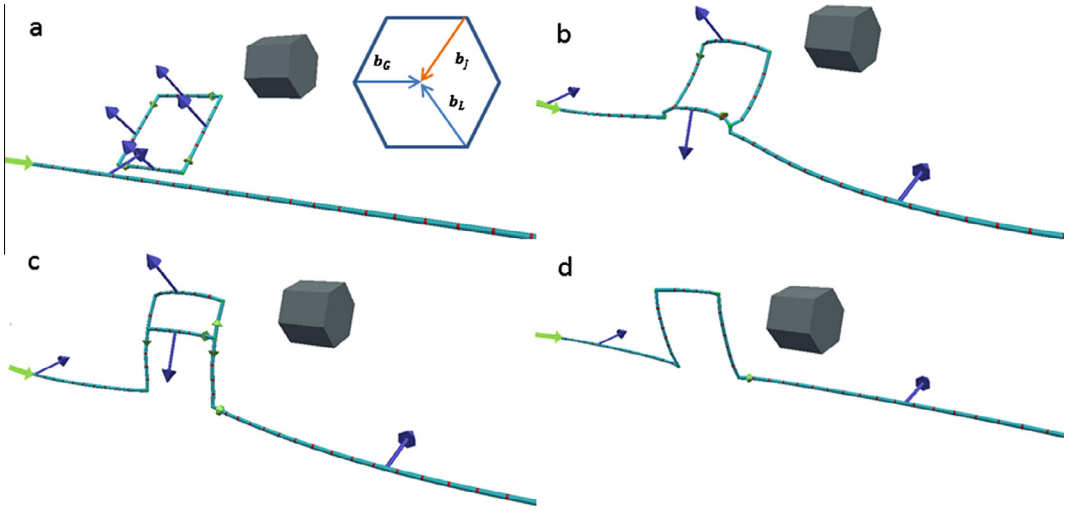

Fig. 3. Interaction between an edge dislocation gliding in a prismatic plane and a loop with a different Burgers vector. The applied resolved shear on the dislocation is $\tau = 100$ MPa. A glissile junction is formed in P_2 with the $\underline{a}_2$ Burgers vector, changing the Burgers vector of the loop and forming a double super-jog on the dislocation line.

prismatic–pyramidal slip systems and collinear annihilation maps for basal–prismatic slip systems, basal–pyramidal slip systems, and prismatic–pyramidal slip systems.

The interaction between a dislocation gliding in the prismatic plane and a loop with different Burgers vector can be interpreted using the prismatic–prismatic interaction map [52] with angles of $\Phi_1 = \Phi_2 = 0°$ for the first stage of the reaction (Fig. 3(b)). In that case, an attractive junction is formed according to the interaction map (see the yellow square in Fig. 4).

When the dislocation interacts with an interstitial loop the same double super-jog is formed. The loop first glides on its cylinder, repelled by the dislocation. Then the dislocation interacts with the opposite side of the loop. Finally, the junction glides in the plane of the loop.

(iii) Screw dislocation gliding in the prismatic plane interacting with a loop with the same Burgers vector

A screw dislocation gliding in the P_1 prismatic plane with a $\underline{b}_G = \underline{a}_1$ Burgers vector interacts with a vacancy loop located in the P_{L1} prismatic plane with a $\underline{b}_L = -\underline{a}_1$ Burgers vector.

Under the applied shear stress ($\tau = 100$ MPa), the dislocation starts to glide. When the dislocation interacts with the loop, it creates a right handed helical turn on the screw dislocation (see Fig. 5). This reaction has been described by Hirsch in the case of FCC metals and in [30] in the case of zirconium. It is referred to as reaction *R*4 in [46], which is defined as the temporary absorption of part or the entire loop into a helical turn on a screw dislocation, and it has been reported previously by several authors [46,72]. The helical turn tends to expand along the dislocation line to lower its energy. The arms of the loop gliding in the basal plane act as strong pinning points for the dislocation glide. The screw dislocation can overcome this type of defect through an Orowan process. As the dislocation segments bow out under the applied stress, it pushes the super-jogs towards each other until both arms of the dislocation join. The dislocation then unpins and leaves behind a perfect prismatic loop. The stress required for this process is very high. However Nogaret et al. [44] have shown that if a second dislocation interacts with the helical turn, a reaction can occur, leading to the emission of a new dislocation in a plane parallel to the initial glide plane of the dislocation. According to these authors, this process probably assists the clear band broadening during tensile loading.

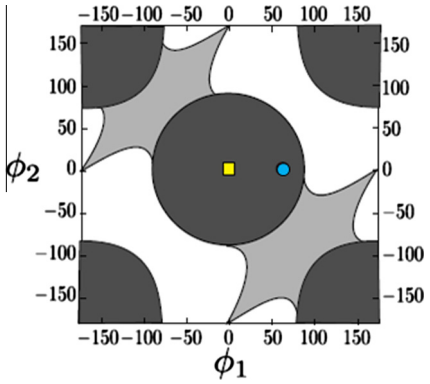

Fig. 4. Schematic of interaction map between two dislocations lying in prismatic planes, dark grey zone is the attractive interaction zone where junctions can form, shaded grey zone corresponds to crossed states formations, and white zone corresponds to repulsive interactions (Adapted from [52–54]). (For interpretation to colours in this figure, the reader is referred to the web version of this paper.)

The similar interaction involving interstitial dislocation loops leads to the formation of a left handed helical turn.

(iv) Screw dislocation gliding in the prismatic plane interacting with a loop with a different Burgers vector

A screw dislocation gliding in the P_1 prismatic plane with a $\underline{b}_G = \underline{a}_1$ Burgers vector interacts with a vacancy loop located in the P_{L3} prismatic plane with a $\underline{b}_L = -\underline{a}_3$.

Under applied shear stress ($\tau = 100$ MPa), the dislocation glides towards the loop, creating a junction at the intersection of the P_1 prismatic plane and the (0001) basal plane, with Burgers vector $\underline{b}_J = \underline{a}_2$ (Fig. 6(b)). Indeed, with the line sense chosen according to Fig. 6, the Burgers vector of the junction is:

$$\underline{b}_J = \underline{b}_L - \underline{b}_G = -\underline{a}_3 - \underline{a}_1 = \underline{a}_2 \quad (4)$$

Based on the prismatic-basal interaction map (Fig. 7), it can be checked that junction formation is favored in this configuration. Indeed, for the dislocation gliding in the P_1 prismatic plane, the angle is $\Phi_1 = 0°$. The arm of the loop, which glides in the basal plane, makes an angle $\Phi_2 = 30°$ with the intersection of the two glide

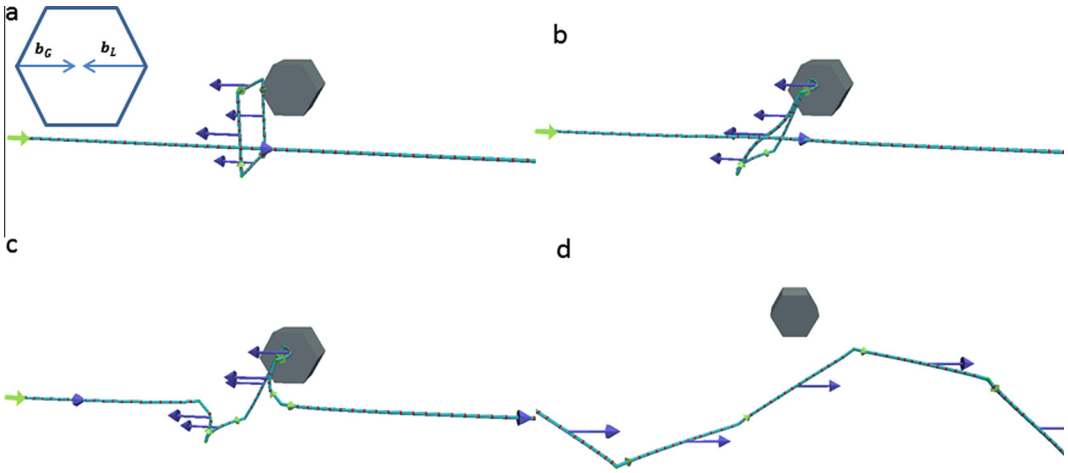

Fig. 5. Interaction between a screw dislocation gliding in a prismatic plane and a loop with the same Burgers vector under constant resolved shear stress (τ = 100 MPa). A helical turn is formed in the $\underline{a}_1$ direction.

planes. For these angles the prismatic–basal interaction map indicates the formation of a junction (blue point in Fig. 7).

This junction pins the dislocation as it cannot glide in the P_1 prismatic plane (Fig. 6(b)). However, two dislocation segments gliding in basal planes appear and propagate on both sides of the loop as shown by the slip plane normal (Fig. 6(b)).

The further glide of the initial Frank-Read source in the P_1 prismatic plane annihilates the created segments in the basal plane at the right of the loop. Indeed, the loop glides along its glide cylinder (going downward in Fig. 6(b)) until its right corner reaches the glide plane of the Frank-Read source. The triple node formed this way is at the intersection of P_1, gliding plane of the dislocation, P_3, gliding plane of the segment of the loop involved in the reaction, and P_2, the habit plane of the new formed junction ($\Phi_2 = 0°$ for the dislocation in P_3 and $\Phi_1 < 90°$ for the dislocation in P_1, see the blue point in Fig. 4). This junction lying in the P_2 prismatic plane has an $\underline{a}_2$ Burgers vector and is therefore able to glide, progressively absorbing the loop on the screw dislocation as a helical turn.

The helical turn then expands along the $\underline{a}_1$ direction. The global result is the formation of an extended helical turn on the gliding dislocation line (*R*4 reaction).

As for the interaction involving a screw dislocation and a loop with same Burgers vectors, the helical turn is a strong pinning point for dislocation glide. This mechanism has been described in details by Hirsch [8] for FCC metals and has been observed in MD simulations performed in nickel [34,36,44]. It is referred as *R*4 reaction in [46].

When the magnitude of applied shear stress is higher than in the previous case (400 MPa), the reaction observed is quite different (Fig. 8). As in the previous case, an attractive junction is formed in the basal plane with $\underline{b}_J = \underline{a}_2$ Burgers vector. Under the applied

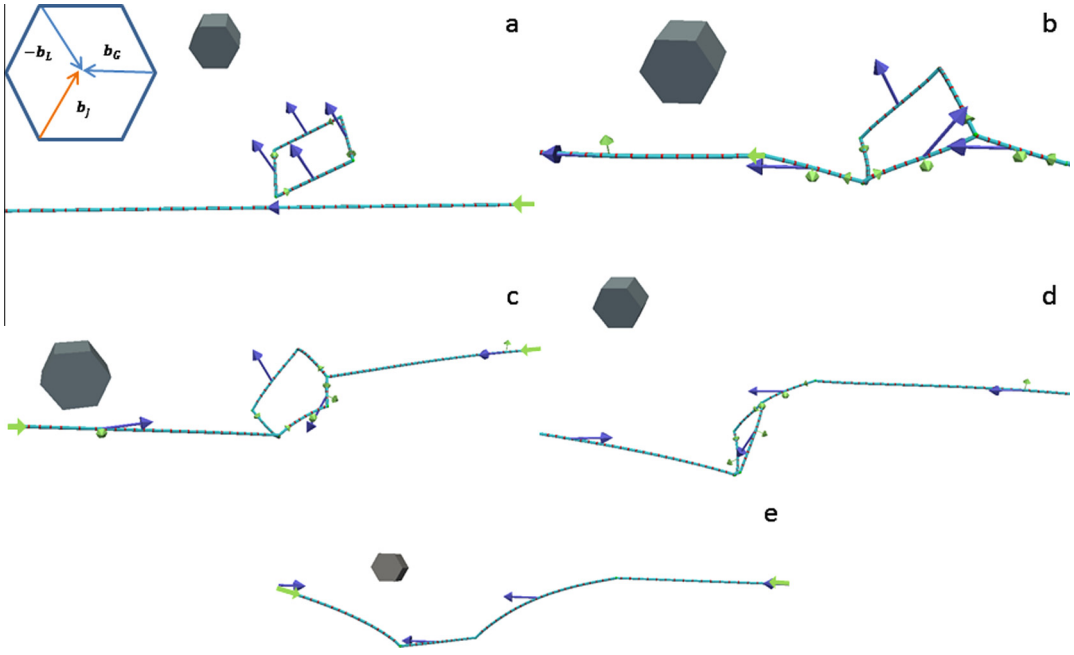

Fig. 6. Interaction between a screw dislocation gliding in a prismatic plane and a loop with a different Burgers vector. The applied stress in the gliding plane of the dislocation is τ = 100 MPa. A glissile junction is formed in the P_2 plane with a $\underline{a}_2$ Burgers vector, which reacts with the loop, changing its Burgers vector into the dislocation Burgers vector.

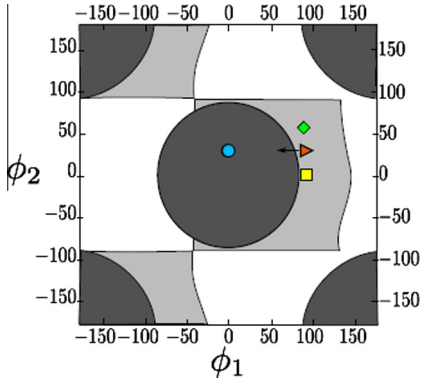

Fig. 7. Schematic of interaction map between a dislocation lying in a prismatic glide system (1) and a dislocation lying in a basal gliding system (2), same color convention as in Fig. 4 (adapted from [53–54]). (For interpretation to colours in this figure, the reader is referred to the web version of this paper.)

shear stress, the gliding dislocation bends, and because of the line tension, the junction shrinks and progressively unzips. The loop is then simply sheared, remaining the same after the glide of the dislocation (Fig. 8(c)). This mechanism is referred as $R1$ reaction in [46] since the loop is crossed by the dislocation but both remain unchanged.

Simulations performed with an interstitial loop, the other parameters remaining equal, show that only for $\tau = 100$ MPa, the dislocation in the P_1 prismatic plane reacts with the second side of the loop located in the basal plane, so that no junction in the P_2 prismatic plane can be formed to further annihilate the loop. The dislocation is nevertheless pinned by the junctions formed in the basal plane.

For higher applied stress ($\tau > 300$ MPa), the junction formed in the basal plane is annihilated and the loop remains unchanged after the interaction.

4.2. Dislocations gliding in a basal plane

The interactions between a loop and a dislocation gliding in the basal plane have also been systematically investigated. Again, edge and screw dislocations with $\underline{b}_G = \underline{a}_1$ Burgers vector gliding in the basal plane (0001) are successively considered.

i. Edge dislocation gliding in the basal plane and interacting with a loop of same Burgers vector

The interaction between an edge dislocation gliding in the basal plane and a loop with the same Burgers vector results in the same reaction as the interaction between an edge dislocation gliding in the prismatic plane and a loop with the same Burgers vector described earlier. This interaction leads to a progressive clearing of loops by dislocations gliding in the basal plane.

ii. Edge dislocation gliding in the basal plane interacting with a loop of different Burgers vector

An edge dislocation gliding in the (0001) basal plane with a $\underline{b}_G = \underline{a}_1$ Burgers vector interacts with a vacancy loop located in the P_{L3} prismatic plane with a $\underline{b}_L = -\underline{a}_3$ Burgers vector (Fig. 9(a)).

Under the applied resolved shear stress ($\tau = 100$ MPa), the dislocation begins to glide toward the loop. The interaction between the dislocation gliding in the basal plane and the vacancy loop leads to the creation of a junction with $\underline{b}_J$ Burgers vector given by Eq. (5), with line directions given in Fig. 9(c).

$$\underline{b}_J = \underline{b}_G - \underline{b}_L = \underline{a}_1 + \underline{a}_3 = -\underline{a}_2 \tag{5}$$

This junction is glissile in the basal plane as its Burgers vector $\underline{b}_J = -\underline{a}_2$ belongs to the basal plane. When pushed by the gliding dislocation, the loop glides along its cylinder Fig. 9(d)). This leads to the clearing of the defect by the glide of the dislocation in the basal plane. This mechanism has been described in details in [26,30]. It is an example of the $R3_{drag}$ mechanism described by Bacon et al. [46] where the obstacle is dragged by the dislocation but both remain unchanged.

The creation of the junction can also be analyzed in terms of prismatic-basal interaction map. Indeed, the dislocation gliding in the basal plane makes an angle of $\Phi_2 = 30°$ with the intersection of the two gliding planes and the arm of the loop in the P_3 prismatic plane makes an angle $\Phi_1 = 90°$. According to the prismatic-basal interaction map, a crossed-state occurs (orange triangle on Fig. 7). However, thanks to the elastic interaction between the dislocation and the loop arm, the dislocation in the prismatic slip system bends towards the dislocation in the basal plane decreasing the angle Φ_1, and allowing the formation of a junction at the intersection of the two planes (Fig. 9 (c)).

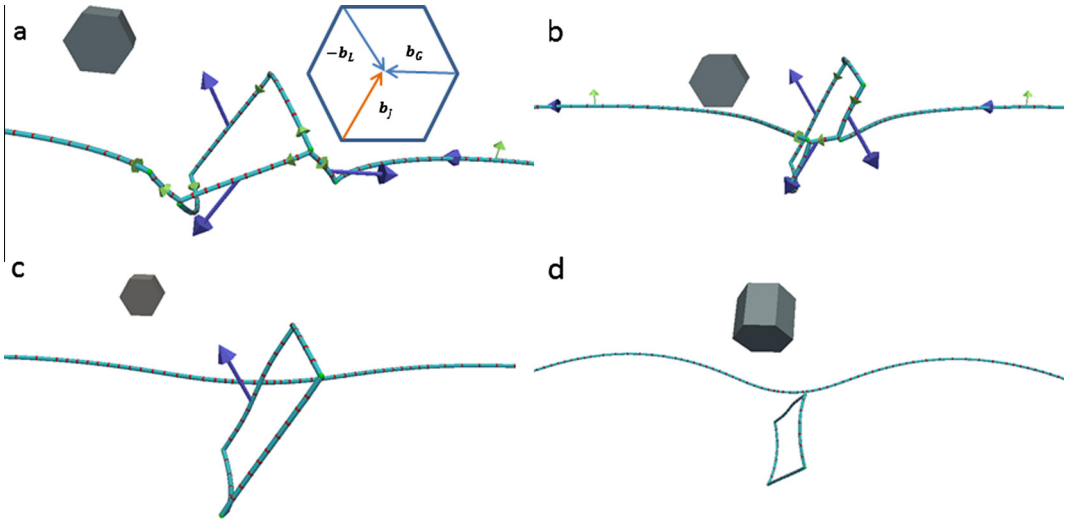

Fig. 8. Interaction between a screw dislocation gliding in a prismatic plane and a loop with a different Burgers vector. The applied resolved shear stress on the dislocation is $\tau = 400$ MPa. The bending of the segments of dislocation around the loop annihilates the new formed junction. This leads to the simple shearing of the loop.

The similar situation involving interstitial loops leads to the same clearing of the defects by formation of a glissile junction in the basal plane.

iii. Screw dislocation gliding in the basal plane interacting with a loop of same Burgers vector

The interaction between a screw dislocation gliding in the basal plane and a loop with the same Burgers vector results in the same reaction as the interaction between a screw dislocation gliding in the prismatic plane and a loop with the same Burgers vector described earlier. This interaction leads to a strong pinning of pure screw dislocations.

iv. Screw dislocation gliding in the basal plane interacting with a loop of different Burgers vector

A screw dislocation gliding in the (0001) basal plane with a $\underline{b}_G = \underline{a}_1$ Burgers vector interacts with a vacancy loop located in the P_{L3} prismatic plane with a $\underline{b}_L = -\underline{a}_3$ Burgers vector (Fig. 10(a)).

Under the applied resolved shear stress ($\tau = 100$ MPa), the screw dislocation glides towards the loop. The dislocation gliding in the basal plane makes an angle $\Phi_2 = 60°$ with the intersection of the two gliding planes, the intersection between B and P_3 planes being along the $\underline{a}_3$ direction. The arm of the loop gliding in the P_3 plane makes an angle $\Phi_1 = 90°$ with the $\underline{a}_3$ direction. According to the prismatic-basal interaction map, a crossed state also occurs (see green rhombus in Fig. 7) in that case (Fig. 10(b)). Nevertheless due to long range elastic interaction, dislocation segments bend, decreasing again the angle Φ_1. A small junction is then formed with a Burgers vector $\underline{b}_J$, given by Eq. (6), with the line directions shown in Fig. 10(b)).

$$\underline{b}_J = -(\underline{b}_G - \underline{b}_L) = -(\underline{a}_1 + \underline{a}_3) = \underline{a}_2 \tag{6}$$

However, this junction remains unstable because the decrease of the angle Φ_1 is too small to enter into the junction formation domain shown on the prismatic-basal interaction map (Fig. 7). Under the applied shear stress, the loop is progressively pushed along its glide cylinder, leading to the clearing of defects by the dislocation gliding in the basal plane.

The similar situation involving interstitial loops leads to the same clearing of the defects by formation of crossed states and gliding of the loops on their glide cylinders.

5. Discussion

The DD computations performed in this study have confirmed the main results of the theoretical analysis described in [30]. However, in the case of an edge dislocation gliding in the prismatic plane interacting with a loop with a different Burgers vector another mechanism than the one proposed in [30] was observed (Fig. 3). Indeed, by taking into account the long range elastic interaction, dislocation segments glide or bend towards each other allowing new mechanisms to occur. The reaction simulated in the case of a screw dislocation gliding in the prismatic plane and interacting with a loop with a different Burgers vector where the loop was unzipped by the junction, changing the Burgers vector of the loop was also hardly foreseen (Fig. 6). Furthermore, the theoretical analysis does not allow predictions of the effect of the applied stress. This shows that DD simulations are of great help to understand the details of elementary interactions between dislocations and irradiation defects.

The present results are also of great help to understand the TEM observations of dislocation channels in neutron irradiated samples made of zirconium alloys and tested at 20 °C or 350 °C [26–29].

The various interactions computed are summarized in Table 1. Table 1 highlights several differences in terms of interactions depending on whether the dislocation glides in the prismatic or in the basal plane, when the Burgers vector of the loop differs from the Burgers vector of the dislocation. The outcome of these reactions for screw dislocations involve the formation of a helical turn in the case of prismatic slip, while the case of basal slip leads to the progressive sweeping of the loop along its glide cylinder thanks to the formation of a glissile junction. These different reactions have various consequences on the following behavior of the gliding dislocation. Considering equal probability (p) of having a loop with one of the three ⟨a⟩ Burgers vectors, the reaction between dislocation and loop with same Burgers vectors occurs with a probability of $p = 1/3$. Since for each configuration, the character of the dislocation, edge or screw, is distinguished, the interaction of a screw dislocation interacting with a loop with the same Burgers vector occurs with a probability of $p = 1/6$. For all the other cases, occurring with a probability of $p = 5/6$, the interaction leads to the clearing or sweeping of the loop.

On the other hand, when the dislocation glides in the prismatic plane, strong pinning occurs for screw dislocations interacting

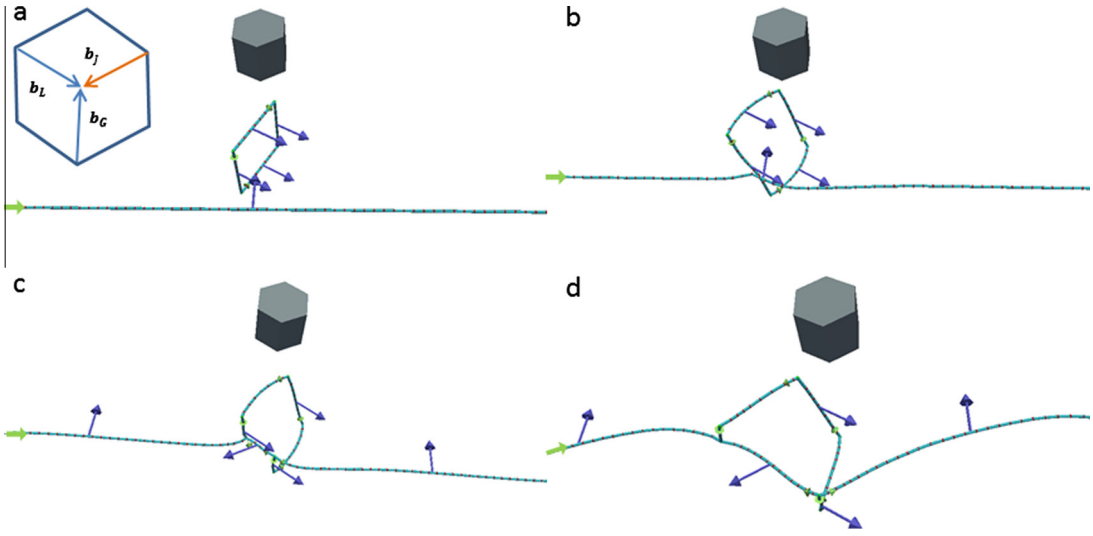

Fig. 9. Interaction between an edge dislocation gliding in the basal plane and a vacancy loop with a different Burgers vector. The formation of a junction with $\underline{b}_J = \underline{a}_2$ Burgers vector allows the glide of the loop along the $\underline{a}_2$ direction.

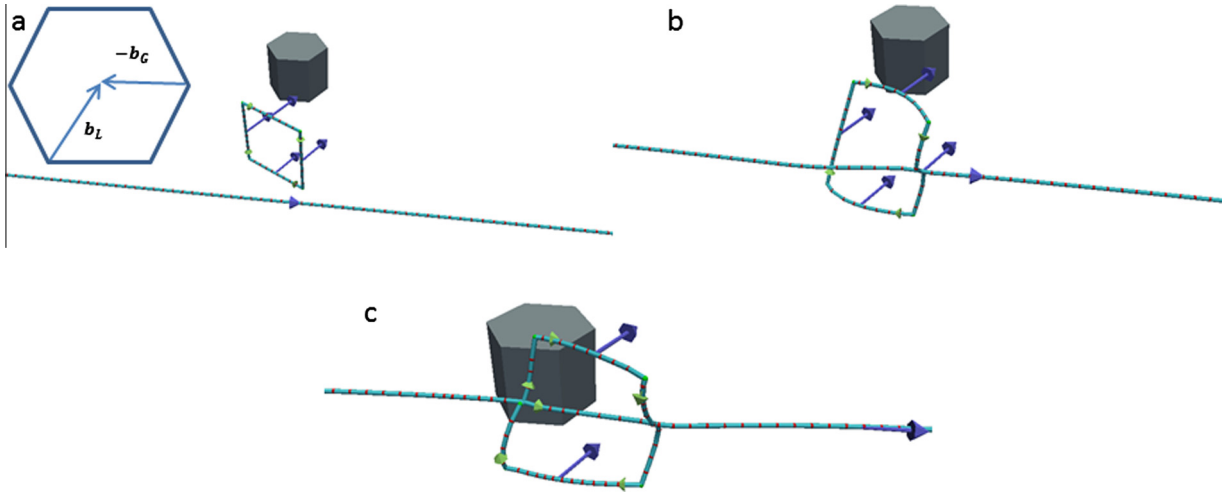

Fig. 10. Interaction between a screw dislocation gliding in the basal plane and a loop with different Burgers vectors. This leads to the progressive clearing of the loop.

Table 1
Summary of the various interactions computed by DD simulations.

	Edge dislocation gliding in the prismatic plane	Screw dislocation gliding in the prismatic plane	Edge dislocation gliding in the basal plane	Screw dislocation gliding in the basal plane
Dislocation and loop with same Burgers vectors ($p = 1/3$)	Double super-jog formation. Clearing of the loop ($R3$)	Helical turn formation. Pinning of the dislocation ($R4$)	Double super-jog formation. Clearing of the loop ($R3$)	Helical turn formation. Pinning of the dislocation ($R4$)
Dislocation and loop with different Burgers vectors ($p = 2/3$)	Double super-jog formation. Clearing of the loop ($R3$)	Helical turn formation. Pinning of the dislocation ($R4$)	Glissile junction formation. Sweeping of the loop ($R3_{drag}$)	Unstable glissile junction formation. Sweeping of the loop ($R1$)

either with loop with same or different Burgers vectors. This corresponds to a probability of $p = 3/6$, the clearing of the loop occurring also with a probability of $p = 3/6$. This shows that strong pinning of dislocation occurs three times more in the case of prismatic glide than in the case of basal glide. This can explain the difficult glide of dislocation in the prismatic plane observed after neutron irradiation whereas before irradiation, the easy slip system is the prismatic slip system. Indeed it has been estimated that the increase of the Critical Resolved Shear Stress (CRSS) due to irradiation is higher for prismatic systems than for basal slip systems [26–29].

Furthermore, this study shows that in five cases over six sweeping or clearing of loops occurs by glide of dislocations in the basal plane whereas this only occurs in three cases over six in the case of dislocations gliding in the prismatic slip. Gliding of loops along their glide cylinder, after interaction with dislocations, therefore occurs mainly in the case of basal slip. This can explain that the dislocation channeling mechanism creating a clear band free of defect occurs more easily in the case of basal slip than in the case of prismatic slip. Moreover, it has been shown by TEM that the clearing seems only partial in the case of prismatic slip whereas a full clearing seems to occur in the case of basal slip [26–30].

These results also show that, in the case of zirconium, the mechanism proposed by Nogaret et al. [58] to explain the clear band formation can also apply. According to these authors, helical turns on screw dislocations is at the heart of the process of clear band formation because jogs created on dislocation by loop incorporation are transported along the dislocation line and also because dislocations can be re-emitted in a parallel glide plane leading to a progressive broadening of the clear band.

At a lower length scale, a good agreement can also be found between the present DD simulations and previous MD simulations obtained on various metals. In many cases, the simulated interactions have already been observed on zirconium [48], and also on nickel [34,36,44] or iron [42]. Contrary to MD simulations, the use of the DD meso-scale method does not allow an accurate description of atomic movements. DD simulations are probably not well suited to compute interactions between dislocations and very small point defect clusters since small atomic displacements can be important in that case but DD simulations become accurate for the computation of interaction with large loops.

DD simulations allow performing large scale simulations involving many loops and many dislocations, typically at the single grain scale [58,59] contrary to MD simulations which are limited to the nanoscale. The space scale reachable with DD simulations is therefore also more representative of the actual microstructure of the material after irradiation.

The reactions observed by DD simulations are also in rather good agreement with in situ observations of interactions between dislocation and irradiation defects in various metals and alloys. Indeed, several authors have observed in a TEM, during in situ tensile testing experiments, the reaction between a gliding dislocation and Stacking Fault Tetrahedron (SFT) in rapidly quenched copper or gold [73–79] or proton irradiated copper [80]. These authors show that SFT act as strong pining point for gliding dislocations but can also collapse by interaction with the gliding dislocation inducing the formation of a double super-jog. Other authors have studied in situ the interaction between dislocation and prismatic loops in rapidly quenched pure aluminum [81], proton irradiated pure molybdenum [82] and austenitic stainless steels [83]. In the case of stainless steels and pure aluminum, the authors have clearly observed unfaulting and incorporation into the dislocation of an intrinsic Frank loop in the form of an helical turn [81,82]. In the case of molybdenum, the authors also observed in situ the clearing of perfect prismatic loops during straining [83].

In a recent study, in situ tensile tests have been performed in a TEM on Zr ion irradiated zirconium alloys [30]. The incorporation of a loop into an edge dislocation gliding in the prismatic plane has been observed during in situ straining, in good agreement with the DD simulations of an edge dislocation gliding in the prismatic plane and interacting with a ⟨a⟩ loop with the same Burgers vector (Fig. 2). Furthermore, a more complex interaction showing the strong pinning of an edge dislocation gliding in a prismatic plane by a loop has also been observed. This reaction cannot be understood with the sole results obtained by these DD simulations since edge dislocation gliding in prismatic plane can always overcome the loop by creating a double super-jog on the dislocation. New in situ experiments on irradiation Zr alloys are also needed in order to gain a better understanding of the elementary interactions in the case of prismatic slip. Moreover, in situ tensile tests where the basal slip is activated would be also very interesting to observe.

From a geometrical point of view, the initial length of the dislocation and the distance between loops play an important role on the value of the typical applied stress needed to activate shearing of the loops. Some simulations performed on non-pure screw or edge but mixed type dislocations have also shown that the resulting mechanism can be significantly modified. More generally, it has been seen that if the initial configuration exhibits some symmetries, specific mechanisms occur but others are inhibited.

As a perspective, to avoid potential artifacts due to the initial geometry of the system, DD simulations could be performed on a large loop population with a variety of positions with respect to the glide plane of the dislocation. Furthermore, in these large scale simulations, dislocations will be mainly of mixed type, with a broad variety of angles between the dislocation line and the Burgers vector. Since on mixed dislocation, the helical turn can be pushed aside, a lower hardening is expected [58]. Also loops of different nature, interstitial or vacancy, or with different Burgers vector could be introduced. This is believed to induce new reactions where right handed helical turn can annihilate left handed helical turn also decreasing the hardening due to helical turns. This type of large scale simulations could then be analyzed using statistical methods, in order to average the influence of the geometry of the elementary interaction.

This discussion shows the importance of performing in the future both advanced DD simulations at individual loop scale to assess more complicated interactions and also at a larger length scale for a better understanding of the channeling process. The constitutive behavior of zirconium single crystal after irradiation is also expected from such massive DD simulations. These constitutive laws could then be eventually introduced into polycrystalline models [29,84] to compute the macroscopic mechanical behavior of neutron irradiated zirconium alloys.

6. Conclusion

A new nodal dislocation dynamics code, NUMODIS, has been used to investigate interactions between gliding dislocations in prismatic or basal planes and dislocation loops in zirconium. The configurations computed here show various mechanisms such as absorption of a loop on an edge dislocation as a double superjog, creation of a helical turn on a screw dislocation, acting as a strong pinning point, and sweeping of a loop by a gliding dislocation. The dislocations gliding in prismatic planes can equally be pinned or lead to the clearing of the loops, whereas for dislocations gliding in the basal plane, most mechanisms lead to the clearing of the loops. This is consistent with the experimental observations of clear bands formation in the basal plane for zirconium alloys observed after neutron irradiation.

Acknowledgements

The authors acknowledge the support of the French Agence Nationale de la Recherche (ANR) under reference ANR-10-COSI-0011 (OPTIDIS) for the numerical development of code NUMODIS. The authors are grateful to the other developers of NUMODIS, M. Blétry, M. Fivel, E. Ferrié, A. Etcheverry and O. Coulaud, and also acknowledge R. Madec for fruitful discussions and explanations. The authors also thank EDF and AREVA for supporting this study.

References

[1] C. Lemaignan, Zirconium Alloys: Properties and Characteristics, vol. 2, in: R. Konings (Ed.), Comprehensive Nuclear Materials, Elsevier Ltd., 2012. Chapter 7.
[2] F. Onimus, J.L. Béchade, Radiation effects in zirconium alloys, vol. 4, in: R. Konings (Ed.), Comprehensive Nuclear Materials, Elsevier Ltd., 2012. Chapter 1.
[3] D.O. Northwood, At. Energy Rev. 15 (4) (1977) 547–610.
[4] A. Jostsons, P.M. Kelly, R.G. Blake, J. Nucl. Mater. 66 (1977) 236–256.
[5] D.O. Northwood, R.W. Gilbert, L.E. Bahen, P.M. Kelly, R.G. Blake, A. Jostsons, P.K. Madden, D. Faulkner, W. Bell, R.B. Adamson, J. Nucl. Mater. 79 (1979) 379–394.
[6] M. Griffiths, J. Nucl. Mater. 159 (1988) 190–218.
[7] P.M. Kelly, R.G. Blake, Philos. Mag. 28 (1973) 415–426.
[8] P.B. Hirsch, Proceedings of a Conference on Point Defect Behavior and Diffusional Processes. University of Bristol, 1976.
[9] G.S. Was, Fundamentals of Radiation Materials Science (Metals and Alloys). Springer Verlag, 2007.
[10] A.J.E. Foreman, Philos. Mag. 17 (146) (1968) 353.
[11] A.J.E. Foreman, J.V. Sharp, Philos. Mag. 19 (1969) 931.
[12] G. Saada, J. Washburn, Proceedings of the international conference on crystal lattice defects. Symp. J. physical society Jpn. 1963, p. 18 (Suppl. 1).
[13] J.L. Strudel, J. Washburn, Philos. Mag. 9 (1964) 491–506.
[14] M.S. Wechsler, The Inhomogeneity of Plastic Deformation, ASM, Metals Park, Ohio, 1973. pp. 19–52.
[15] J.V. Sharp, Philos. Mag. 16 (1967) 77–96.
[16] J.V. Sharp, Radiat. Effects 14 (1972) 71.
[17] M.J. Makin, Philos. Mag. 21 (1970) 815–821.
[18] A. Luft, Prog. Mater. Sci. 35 (1991) 97–204.
[19] C.E. Coleman, D. Mills, J. van der Kuur, Can. Metall. Quaterly 11 (1972) 91–100.
[20] C.D. Williams, R.B. Adamson, K.D. Olhausen, European Conference on irradiation behavior of fuel cladding and core component materials. Karlsruhe, 1974, pp. 189–192.
[21] T. Onchi, H. Kayano, Y. Higashiguchi, J. Nucl. Mater. 88 (1980) 226–235.
[22] K. Pettersson, J. Nucl. Mater. 105 (1982) 341–344.
[23] R.B. Adamson, W.L. Bell, International Symposiums, vol. 1, Xian, China, 1985, pp. 237–246.
[24] M. Fregonese, C. Régnard, L. Rouillon, T. Magnin, F. Lefebvre, C. Lemaignan, ASTM STP 1354 (2000) 377–398.
[25] C. Régnard, B. Verhaeghe, F. Lefebvre-Joud, C. Lemaignan, ASTM STP 1423 (2002) 384–399.
[26] F. Onimus, I. Monnet, J.L. Béchade, C. Prioul, P. Pilvin, J. Nucl. Mater. 328 (2004) 165–179.
[27] F. Onimus, J.L. Béchade, C. Prioul, P. Pilvin, I. Monnet, S. Doriot, B. Verhaeghe, D. Gilbon, L. Robert, L. Legras, J.-P. Mardon, J. ASTM Int. 2 (8) (2005).
[28] B. Bourdiliau, F. Onimus, C. Cappelaere, V. Pivetaud, P. Bouffioux, V. Chabretou, A. Miquet, J. ASTM Int. 7 (9) (2010).
[29] F. Onimus, J.L. Béchade, D. Gilbon, Metall. Mater. Trans. A 44A (2013) 45–60.
[30] F. Onimus, L. Dupuy, F. Mompiou, Prog. Nucl. Energy 57 (2012) 77–85.
[31] D. Rodney, G. Martin, Phys. Rev. Lett. 82 (16) (1999).
[32] D. Rodney, G. Martin, Phys. Rev. B 61 (13) (2000).
[33] D. Rodney, G. Martin, Y. Bréchet, Mater. Sci. Eng. A309–310 (2001) 198–202.
[34] D. Rodney, Acta Mater. 52 (2004) 607–614.
[35] D. Rodney, C. R. Phys. 9 (2008) 418–426.
[36] D. Rodney, Nucl. Instrum. Methods Phys. Res. B 228 (2005) 100–110.
[37] Y.N. Osetsky, D.J. Bacon, Mater. Sci. Eng., A 400–401 (2005) 374–377.
[38] Y.N. Osetsky, R.E. Stoller, D. Rodney, D.J. Bacon, Mater. Sci. Eng., A 400–401 (2005) 370–373.
[39] Y.N. Osetsky, D. Rodney, D.J. Bacon, Philos. Mag. 86 (16) (2006) 2295–2313.
[40] L. Saintoyant, H.-J. Lee, B.D. Wirth, J. Nucl. Mater. 361 (2007) 206–217.
[41] S. Jumel, J.-C. Van Duysen, J. Ruste, C. Domain, J. Nucl. Mater. 346 (2005) 79–97.
[42] Z. Rong, D. Bacon, Y. Osetsky, Mater. Sci. Eng., A 400–401 (2005) 378–381.
[43] D.J. Bacon, Y.N. Osetsky, Z. Rong, Philos. Mag. 86 (25–26) (2006) 3921–3936.
[44] T. Nogaret, C. Robertson, D. Rodney, Philos. Mag. 87 (6) (2007) 945–966.
[45] E. Martinez, J. Marian, A. Arsenlis, M. Victoria, J.M. Perlado, Philos. Mag. 88 (6, 21) (2008) 809–840.
[46] D.J. Bacon, Y.N. Osetsky, D. Rodney, Dislocation–obstacle interactions at the atomic level, in: J.P. Hirth, L.P. Kubin (Eds.), Dislocations in Solids, Elsevier B.V., 2009.
[47] Y.N. Osetsky, D.J. Bacon, Atomic-level dislocation dynamics in irradiated metals, vol. 1, in: R. Konings (Ed.), Comprehensive Nuclear Materials, Elsevier Ltd., 2012.

[48] R.E. Voskoboynikov, Yu.N. Osetsky, D.J. Bacon, Mater. Sci. Eng. A 400–401 (2005) 54–58.
[49] R.E. Voskoboynikov, Yu.N. Osetsky, D.J. Bacon, Mater. Sci. Eng. A 400–401 (2005) 49–53.
[50] G.J. Ackland, S.J. Wooding, D.J. Bacon, Philos. Mag. A 71 (1995) 553.
[51] A. Serra, D.J. Bacon, Modell. Simul. Mater. Sci. Eng. 21 (2013).
[52] G. Monnet, B. Devincre, L.P. Kubin, Acta Mater. 52 (2004) 4317–4328.
[53] C. Wu, S. Aubry, P. Chung, A. Arsenlis, Proceedings of the MRS Fall 2011 Conference, Boston, 2011.
[54] B. Devincre, Philos. Mag. 93 (1–3) (2013) 235–246.
[55] J. Chevy, F. Louchet, P. Duval, M. Fivel, Philos. Mag. Lett. 92 (6) (2012) 262–269.
[56] T.D. de la Rubia, H.M. Zbib, T.A. Khraishi, B.D. Wirth, M. Victoria, M.J. Caturla, Lett. Nat. 406 (24) (2000).
[57] N.M. Ghoniem, S.-H. Tong, B.N. Singh, L.Z. Sun, Philos. Mag. A 81 (11) (2001) 2743–2764.
[58] T. Nogaret, D. Rodney, M. Fivel, C. Robertson, J. Nucl. Mater. 380 (2008) 22–29.
[59] A. Arsenlis, M. Rhee, G. Hommes, R. Cook, J. Marian, Acta Mater. 60 (2012) 3748–3757.
[60] V.V. Bulatov, W. Cai, Computer Simulations of Dislocations, Oxford University Press, Oxford, 2006.
[61] V.V. Bulatov, W. Cai, Phys. Rev. Lett. 89 (11) (2002).
[62] A. Arsenlis, W. Cai, M. Tang, M. Rhee, T. Oppelstrup, G. Hommes, T.G. Pierce, V.V. Bulatov, Mater. Sci. Eng. 15 (2007) 553–595.
[63] W. Cai, C. Weinberger, V.J. Bulatov, Mech. Phys. Solids 54 (2006) 561–587.
[64] G.J.C. Carpenter, Scr. Metall. 10 (1976) 411–413.
[65] J. Ribis, F. Onimus, J.-L. Béchade, S. Doriot, A. Barbu, C. Cappelaere, C. Lemaignan, J. Nucl. Mater. 403 (2010) 135–146.
[66] D.O. Northwood, H.E. Rosinger, J. Nucl. Mater. 89 (1980) 147–154.
[67] E.B. Schwenk, K.R. Wheeler, G.D. Shearer, R.T. Webster, J. Nucl. Mater. 73 (1978) 129–131.
[68] R. Madec, B. Devincre, L. Kubin, T. Hoc, D. Rodney, Science 301 (2003) 1879–1882.
[69] L.K. Wickham, K.W. Schwarz, J.S. Stölken, Phys. Rev. Lett. 83 (22) (1999) 4574–4577.
[70] W. Püschl, Phys. Stat. Sol. A 90 (1985) 181.
[71] R. Madec, B. Devincre, L.P. Kubin, Comput. Mater. Sci. 23 (2002) 219–224.
[72] J.P. Hirth, J. Lothe, Theory of Dislocations, second ed., Wiley, New York, 1982.
[73] M. Briceño, J. Kacher, I.M. Robertson, J. Nucl. Mater. 433 (2013) 390–396.
[74] Y. Matsukawa, G.S. Liu, J. Nucl. Mater. 425 (2012) 54–59.
[75] J.S. Robach, I.M. Robertson, B.D. Wirth, A. Arsenlis, Philos. Mag. 83 (8) (2003) 955–967.
[76] Y. Matsukawa, S.J. Zinkle, J. Nucl. Mater. 329–333 (2004) 919–923.
[77] Y. Matsukawa, Y.N. Osetsky, R.E. Stoller, S.J. Zinkle, Mater. Sci. Eng. A 400–401 (2005) 366–369.
[78] Y. Matsukawa, Y.N. Osetsky, R.E. Stoller, S.J. Zinkle, J. Nucl. Mater. 351 (2006) 285–294.
[79] J.S. Robach, I.M. Robertson, H.-J. Lee, B.D. Wirth, Acta Mater. 54 (2006) 1679–1690.
[80] R. Schäublin, Z. Yao, P. Spätig, M. Victoria, Mater. Sci. Eng., A 400–401 (2005) 251–255.
[81] J.-L. Strudel, J. Washburn, Philos. Mag. 9 (1964) 491–506.
[82] M. Suzuki, A. Fujimura, A. Sato, J. Nagakawa, N. Yamamoto, H. Shiraishi, Philos. Mag. A 64 (2) (1991) 395–411.
[83] M. Suzuki, A. Sato, T. Mori, J. Nagakawa, N. Yamamoto, H. Shiraishi, Philos. Mag. A 65 (6) (1992) 1309–1326.
[84] F. Onimus, J.-L. Béchade, J. Nucl. Mater. 384 (2009) 163–174.